Medical & Biological Engineering & Computing
https://doi.org/10.1007/s11517-019-02071-1

ORIGINAL ARTICLE

Nucleus and cytoplasm–based segmentation and actor-critic neural network for acute lymphocytic leukaemia detection in single cell blood smear images

Krishna Kumar Jha[1] · Himadri Sekhar Dutta[2]

Received: 23 February 2019 / Accepted: 5 November 2019

Abstract
Acute lymphoblastic leukaemia (ALL), which is due to the malfunctioning in the bone marrow, is common among people all over the world. The haematologist suffers a lot to discriminate the presence of leukaemia in the patients using the blood smears. To overcome the inaccuracy and reliability issues, this paper proposes an automatic method of leukaemia detection, named chronological Sine Cosine Algorithm–based actor-critic neural network (Chrono-SCA-ACNN). Initially, the blood smear images are segmented using the proposed entropy-based hybrid model, from which the image-level features and statistical features are extracted from the segments. Then, the selected features are applied to the proposed classifier, which detects the leukaemia. In the proposed Chrono-SCA-ACNN, the optimal weights are selected by the proposed Chrono-SCA, which is the integration of the chronological concept in the SCA. Finally, the experimentation is performed using the ALL-IDB2 database, and the effectiveness of the proposed method over the existing methods is evaluated. From the analysis, the accuracy of the proposed method is found to be 0.99, which proves that it outperforms the existing classification methodologies.

Keywords Blood smear images · Actor critic neural network · Leukaemia detection · Fuzzy C-means · Sine Cosine Algorithm

1 Introduction

With the advent of digital microscopic imaging, image processing and decision support systems, data analysis and classification emerges as a significant method for diagnostic research [1, 2]. At present, computer technology and artificial intelligence are the major steps in the diagnosis of the diseases [3, 4]. Physicians keenly note the internal structures [5] and abnormalities of the cells through effective visualization and the analysis of the images [1]. Microscopic analysis of blood appears to be a significant step in medical diagnosis [6, 7] that identifies the blood-related diseases [8]. The microscope inspection of blood smears is progressed through the counting of various types of white blood cells (WBCs), and that is often progressed using the blood tests by haematologists [9, 10]. However, counting the number of WBCs or leukocytes in the peripheral blood is the significant step that helps the pathologists to diagnose the diseases, like leukaemia and the associated blood diseases. In general, WBCs are classified as eosinophils, basophils, neutrophils, monocytes and lymphocytes, and the counting is performed manually or automatically. The manual procedure of counting offers better recognition rate but consumes more time and exhibits non-standard accuracy; moreover, the accuracy depends on the skills of the operator. Hence, the automatic method to count the WBCs appears to be effective in the computer-aided diagnosis system [3].

The significant steps in the automatic WBC recognition system are as follows: The first step is the detection of the WBCs from the peripheral blood image, the second step is the extraction of the effective features from the detected RBCs and the third step is to model the classifier [3, 9]. The techniques employed for segmentation and classification fall under four major categories, namely threshold, boundary, region and hybrid. Most of the techniques use the combination of boundary and region as criteria [11]. Threshold-based methods, like Otsu and histogram [12, 13], segment the WBCs from the blood smear image based on their intensity

✉ Krishna Kumar Jha
kkjha.visual@gmail.com

[1] Calcutta Institute of Technology, Banitabla, Uluberia, Howrah – 711316, India

[2] Kalyani Government Engineering College, Kalyani, West Bengal, India

Published online: 06 December 2019

level. Contour-based methods determine the nucleus boundary with irregularities [12] along with selective filtering [9] and segment leukocytes from other blood components. The region and hybrid segmentations use the multi-resolution analysis for unsheathing the expected region [9] in order to identify the nucleus and cytoplasm of the WBCs. The colour image segmentation exhibits highly reliable image segmentation with respect to the grey-level images [14]. The blast count is obtained from the peripheral blood, and bone marrow aspirate smears either morphologically or through the core biopsy using the immunohistochemical staining [15] method [16]. The presence of an unexpected number of blast cells in the peripheral blood appears as a symptom of leukaemia [17].

Leukaemia is a blood disease that originates from the bone marrow, producing a huge number of malignant and immature WBCs [17]. There are four types of leukaemia, among which acute lymphoblastic leukaemia (ALL) is a significant one [1, 18, 19]. ALL is due to the overproduction of lymphoblasts in the bone marrow, as a result of which the human body fails to fight with pathogens, causing death. Usually, the haematopoietic disorder prevails among the group of children aged 2–5 years and in adults of age more than 50 years. Diagnosis is categorized with the identification and classification of WBCs, and the presence of the uncontrolled number of blast cells in WBCs initiates various developmental phases of lymphoblastic leukaemia [20]. Some of the standard treatments are chemotherapy and radiotherapy [21]. The standard classification methods to classify ALL are the World Health Organization (WHO) and French–American–British (FAB). According to the FAB classification, there are three subtypes of ALL, such as L1, L2 and L3, which depend on the morphological structure of the cell [9]. Based on the visual inspection and information offered by haematopathologist, the size and shape of the acute leukemic cells are irregular that are invisible in the microscopic examination. Hence, it is a tedious role for the haematologist to predict ALL in advance due to their rapid expansion in stem cell [19].

This paper proposes the leukaemia classification model using the actor-critic neural network (ACNN). Leukaemia detection using the blood smear images is an advancing trend that segments the cytoplasm and nucleus from the input image and progresses the classification. Initially, the blood smear image is pre-processed for enhancing the quality of the image, and the pre-processed image is subjected to the segmentation process using the proposed entropy-based hybrid model. The hybrid model is based on the active contour and fuzzy C-means (FCM) that depends on the entropy parameter. The segments extracted from the image are allowed for the feature extraction that ensures the dimensionally reduced set of features. The features are presented for the classification using the ACNN, and the weights of the ACNN are tuned optimally using the proposed chronological Sine Cosine Algorithm (Chrono-SCA). The classification using the proposed classification model is accurate and improves the effectiveness of the classification.

The major contributions of the paper are as follows:

- *Proposed entropy-based hybrid model for segmentation*: The segmentation of the interested area from the image is obtained using the entropy-based hybrid model. The hybrid model uses the active contour and FCM, and the segments are generated based on the entropy parameter.
- *Proposed Chrono-SCA*: The proposed Chrono-SCA is the integration of chronological concept in the SCA that aims at tuning the optimal weights of the ACNN.

The paper is organized as follows: Section 1 deliberates the background of the paper, and Section 2 presents the motivation to the work. The proposed method of leukaemia classification is discussed in Section 3, and the results and discussion of the proposed method of classification are deliberated in Section 4. Finally, Section 5 concludes the paper.

2 Related works

This section discusses the existing leukaemia detection techniques with their merits and demerits. Khashman and Abbas [18] developed an identification method using a neural network that detects ALL. The method offered less computational time and cost without the use of segmentation and local feature extraction steps, but the method failed to find the other three common types of leukaemia. Rawat et al. [19] introduced the classification strategy of ALL, for which the hybrid hierarchical classifiers are employed. The method appeared to be efficient and robust, and it strongly supported the medical application through the advance identification of lymphoblast cancerous cell; however, the method was ineffective for a bigger database. Srisukkham et al. [22] employed the barebones particle swarm optimization (BBPSO) algorithm for detecting leukaemia that offered better diversification for the search process and minimized the premature convergence of the original BBPSO algorithm, but it was inapplicable to other medical datasets. Li et al. [9] employed the segmentation method using the dual-threshold method that used the combination of RGB and hue, saturation and value (HSV) colour space. The method offered better accuracy, the performance of the proposed method was better when compared with the single-threshold approach independently performed in RGB and HSV colour space and the method was robust. The demerit of the method is that the separation of the whole WBC, including the nucleus and cytoplasm from the image, is a challenge. Zhao et al. [3] employed the convolutional neural networks for automatic classification and detection of leukocytes. The method was better than the iterative threshold method, offering less cost and time. It cannot detect all the

WBCs for some peripheral images, and it sometimes regards a few non-WBCs as WBCs. Mishra et al. [8] proposed the detection strategy that offered greater segmentation and classification accuracy, but not applicable to acute myeloid leukaemia (AML) and subclassification of ALL. Viswanathan [23] used fuzzy C-means for detecting the leukaemia, for which the morphological contour segmentation strategy was used. The algorithm offered better accuracy, and the time of consumption was low when compared to normal haematologist's visual classification. However, the detection performance is poor in case of poor contrast.

2.1 Challenges

- Automatic WBC segmentation is the significant step in automatic blood cell morphology analysis, and it is a hectic challenge due to the morphological diversity and the complex background of blood microscopic images of WBCs [9].
- The automated systems depend on the features, like Hausdorff dimension and cell energy that classify the cancer cells, but the method suffers from the segmentation errors as a result of the similar grey-level and texture features obtained from the interested objects. The above problem is resolved using the supervised learning technique but needs the essential set of training samples to train the network [23].
- There is a problem in the diagnostic step, which causes issues related to the similar signs [18] and, moreover, suffers from the complexity associated with blood smear images. Therefore, the change in slide preparation techniques requires extensive work so as to attain the demands of real clinical issues [23].
- The robust and efficient computerized diagnosis is based on the identification of the characteristics of the healthy and blast cells. There are numerous studies to separate and obtain the nucleus and cytoplasm or only the nuclei of the blood cell, but there is no effective method to select the significant discriminative characteristics from the segmented regions such that it ensures the ALL diagnosis [22].
- A hybrid hierarchical classification method is presented in [19] to segment the microscopic blood image as regions for detecting ALL, but the accuracy is poor.

3 Leukaemia detection based on the proposed segmentation and classification using the entropy-based hybrid model and Chrono-SCA-ACNN

The main aim of the paper is to segment and classify the WBCs for ALL detection in single cell blood smear images. Initially, the blood smear image is subjected to pre-processing in order to enhance the quality of the input image so as to make it effective for the further processes associated with leukaemia detection. The pre-processed image is applied to the segmentation process that segments the cytoplasm and nucleus using the entropy-based hybrid model. The entropy-based hybrid model is developed using the FCM and active contour to segment the cytoplasm and nucleus that is fused using the entropy. The segments are subjected to the feature extraction that extracts the statistical features and the colour histogram–based features from the segments. The features are presented to the ACNN, and the weights of the neural network (NN) are optimally tuned using the proposed Chrono-SCA. The block diagram of the proposed method of leukaemia detection is depicted in Fig. 1.

Consider the blood smear database (d) that consists of the m number of images, represented as

$$d = \{J_1, J_2, ..., J_j, ..., J_m\} \tag{1}$$

where J_j denotes the jth image and there is m number of images in the database.

3.1 Pre-processing phase

Pre-processing makes the image reliable for analysis and enhances the quality of the image so as to facilitate effective segmentation. The enhanced image is resized to reduce the complexity of the classification. Then, the pre-processed image is subjected to the segmentation process that ensures effective processing.

3.2 Proposed entropy-based hybrid model for segmentation

The section presents the segmentation using the proposed hybrid model that is based on entropy factor through the comparison of the segments generated using the active contour model and FCM. The segmentation is progressed to concentrate on the nucleus and the cytoplasm of the cell such that the nucleus and cytoplasm are the points of interest that facilitate the leukaemia detection effectively. The changes in the nucleus and cytoplasm of the cell in terms of their characteristics and shape inherit the presence or absence of leukaemia.

3.2.1 Active contour-based model

The object in the image is detected using the region-based model, named as Chan–Vese model [24]. Initially, the image is subdivided as a number of regions, and each region is presented as a piece-wise constant. The curve is the initial contour that detects the objects in the image, and the main concept behind the contour is that it divides the image into separate

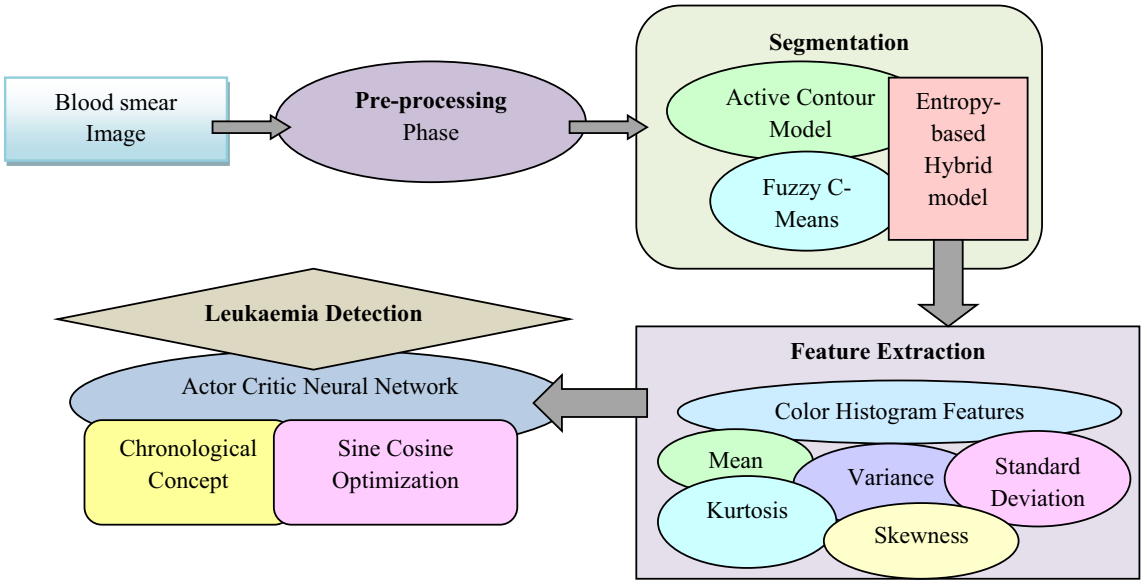

Fig. 1 Block diagram of the proposed leukaemia detection

portions. The two divided portions are a portion inside the curve and a portion outside the curve. Each of the portions of the image is represented as τ, which is the average of the pixel values in that region. For fitting the curve over the object in the image, the minimal variation of the pixel intensities in and out of the image is noted. One can say that the curve fitting over an object in the image is the minimization problem that shows the minimum variation of the intensities in and out of the curve. The time motion of the curve is represented as

$$\frac{\partial \psi}{\partial t} = \lambda_{\vartheta}(\psi)\left[\sigma\, div\, \frac{\nabla\psi}{|\nabla\psi|} - \gamma - \delta_1.\left(J_j - \tau_1\right)^2 + \delta_2.\left(J_j - \tau_2\right)^2\right] \tag{2}$$

where τ and σ are the scaling factors and δ_1 and δ_2 are the weighing parameters. Let the image be J_j and τ is a constant. The scaling parameter σ denotes the length of the curve in terms of the curvature, and the small values of σ signifying that the length of the curve are large, enabling the detection of small objects and holes. On the other hand, the larger values of σ symbolize that the length of the curve cannot be extended such that the larger objects can be detected from the image. The area of the curve is decided using the scaling parameter τ, and the weighing constants represent the forces inside and outside the curve. Thus, the two active regions segmented using the active contour are the cytoplasm and nucleus from the input image. The segments extracted using the active contour are represented as S^a.

3.2.2 Fuzzy C-means clustering

The fuzzy C-means algorithm [23] is the unsupervised clustering algorithm, and the main aim of the algorithm is to extract the segments of interest from the input image. The initial step is the random generation of the cluster centres, and then, the fuzzy membership is computed followed by the calculation of the fuzzy centres. The iteration is repeated until the difference between the minimization function of the current and the previous iterations lies below the threshold. The merits of FCM in performing the segmentation is that the method offers better results for the overlapped data and functions better than the k-means algorithm. The membership is assigned to the individual cluster due to which the data point belongs to more than a cluster. Let us denote the u number of objects given as $(y_1, y_2, ..., y_i, ...y_u)$ in R-dimensional space with fuzzy clusters given as

$$C = \{C_1, C_2, ..., C_h, ..., C_z\} \tag{3}$$

The objective function aims at the minimization problem and is given as

$$M_{\mu} = \sum_{i=1}^{q}\sum_{h=1}^{r} v_{ih}^{\mu} \times D_{ih} \tag{4}$$

where $D_{ih=} = \|y_i - C_h\|$. Initialize the membership function that is denoted as v_{ih}, where $i = 1, 2, ..., u$ and $j = 1, 2, ..., z$ and compute the cluster centres in the second step. The centroid of the hth cluster is computed as

$$C_h = \frac{\sum_{i=1}^{u} v_{ih}^{\mu}.y_i}{\sum_{i=1}^{u} v_{ih}^{\mu}} \tag{5}$$

The process is repeated until the required segments are extracted from the input image. The segments extracted using the FCM is represented as S^f.

3.2.3 Proposed entropy-based hybrid model

The entropy-based hybrid model is employed for the segmentation of the image into segments based on the entropy parameter. The segments of the image are obtained based on the following formula:

$$S_{k,l} = \begin{cases} S^a_{k,l} & ; \quad \text{if } S^a_{k,l} == S^f_{k,l} \\ L & ; \quad \text{if } S^a_{k,l} \neq S^f_{k,l} \end{cases} \tag{6}$$

The segments obtained using the active contour and FCM are compared, and if the pixels in the image belong to the same segment, the segment remains the same. In case the particular pixel of the image obtained using active contour and FCM differs, the entropy of the segment with respect to the neighbouring pixels is computed. The segments corresponding to the minimum entropy are chosen for generating the segment of the image.

The entropy of the pixel centred at (k, l) computed using the active contour model is calculated as

$$L_1 = \text{Entropy}\left(S^a_N(k,l)\right) \tag{7}$$

where S^a_N is the neighbour of S^a. The entropy of the pixel centred at (k, l) computed using the FCM is calculated as

$$L_2 = \text{Entropy}\left(S^f_N(k,l)\right) \tag{8}$$

$$L = \begin{cases} S^a_N(k,l) & ; \quad \text{if } L_1 < L_2 \\ S^f_N(k,l) & ; \quad \text{else} \end{cases} \tag{9}$$

- *Step 1: Read the segments obtained using active contour and FCM*: The segments generated using the active contour and FCM are read by the hybrid model.
- *Step 2: Compute the entropy of individual segments*: The segment to which the individual pixels of the image belong that is identified using the active contour and FCM is compared. If the segment id of the corresponding pixel is the same, the segments are updated; otherwise, the entropy of the pixels for the individual models is computed, and the pixel that responds with the minimum value of the entropy is updated.
- *Step 3: Update the segment of the image*: The entropy of the pixel with the minimum value is updated as the segment of the image. The segment number of the image represents whether the segment is a nucleus, cytoplasm or outer area of the image. Figure 2 represents the entropy-based hybrid model developed for segmentation.

3.3 Image-based and segment-based features for classification

The features extracted from the segment are highlighted in this section. The image-level features include the colour histogram features that facilitate the effective recognition of leukaemia. The statistical-based features include the mean, variance, standard deviation, kurtosis and skewness that indicate the texture of the segments and improve the accuracy of the classification. The importance of feature extraction is that the highly significant information is unsheathed from the image such that the dimensional reduction is achieved that releases the complexity associated with the classification.

3.3.1 Colour histogram features

The colour histogram [25] shows the colour distribution of the image and the part of the image that accompanies the corresponding colour. For the large-sized image, pixels are subdivided as bins yielding the histogram, which is the intensity distribution of the image. The application of the histogram to the image is depicted in the following equation:

$$F_1^{\kappa,\mathfrak{R}} = \left[H_G^{\text{red}} \;\; H_G^{\text{green}} \;\; H_G^{\text{blue}}\right] = H\left[S^{\mathfrak{R}}_{j,\kappa}\right] \tag{10}$$

such that $\kappa \in \{1, 2\}$ and $\mathfrak{R} \in \{a, f\}$.

In Eq. (10), $H\left[S^{\mathfrak{R}}_{j,\kappa}\right]$ is the colour histogram of the κth segment belonging to the jth image, and the histogram probabilities of red, green and blue images are denoted as H_G^{red}, H_G^{green} and H_G^{blue}, respectively. The histogram probability is denoted as

$$H_G = \frac{|S_G|}{\left|S^{\mathfrak{R}}_{j,\kappa}\right|} \tag{11}$$

The range of the grayscale values is given as $[0 \leq G \leq 255]$. The histogram probability is denoted as H_G. $|S_G|$ is the total number of pixels in the grayscale, and $\left|S^{\mathfrak{R}}_{j,\kappa}\right|$ denotes the total number of pixels in the κth segment belonging to the $\mathfrak{R}$th model of the jth image. The dimension of the individual histogram probability is given as $(\chi \times 3)$, and χ is the total number of bins.

$$H_G^{\text{red}} = S_G^{\text{red}} \tag{12}$$

$$H_G^{\text{green}} = S_G^{\text{green}} \tag{13}$$

$$H_G^{\text{blue}} = S_G^{\text{blue}} \; (0 \leq G \leq 255) \tag{14}$$

where G indicates the total number of pixels in the grayscale.

3.3.2 Mean

Mean is the statistical feature and is computed by taking the average of the pixels of the individual segment. It is given as

$$F_2^{\kappa,\mathfrak{R}} = \eta = \frac{1}{p} \times \sum_{b=1}^{P} S^{\mathfrak{R},P}_{j,\kappa} \tag{15}$$

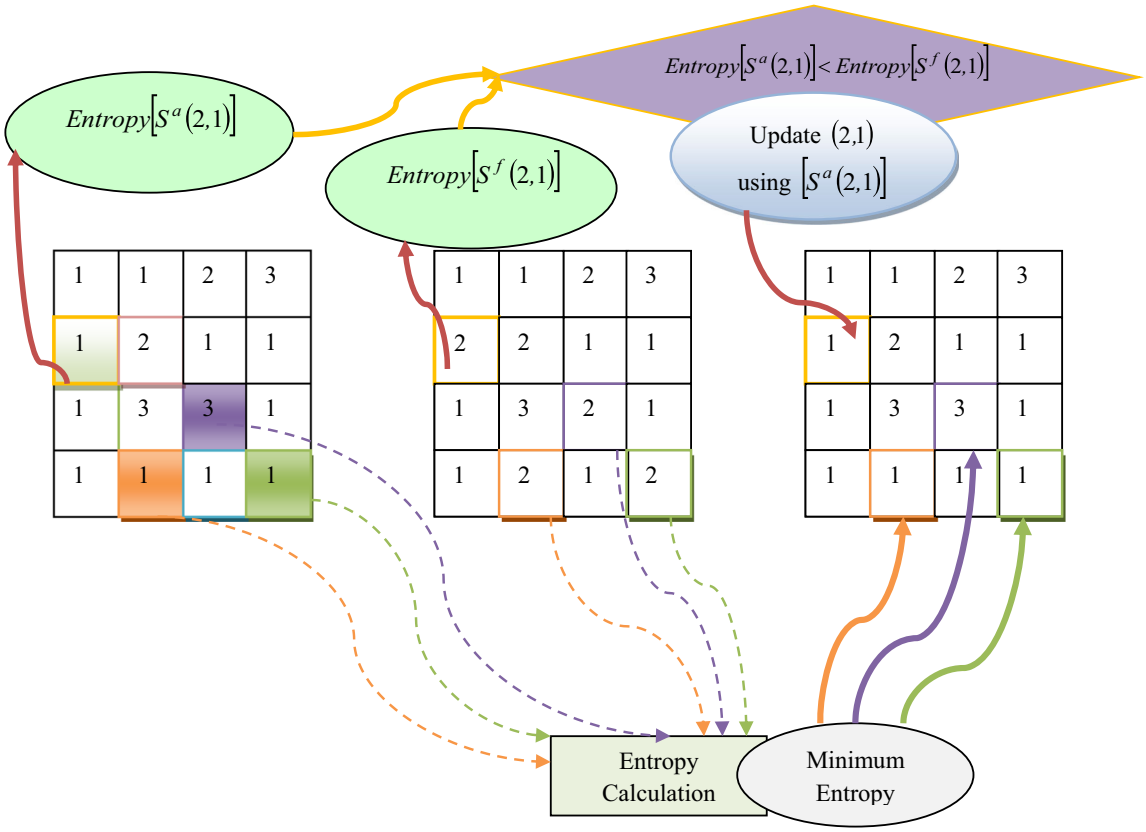

Fig. 2 Proposed entropy-based hybrid model for segmentation

The dimension of P is denoted as $(\exists_1 \times \exists_2)$, $S_{j,\kappa}^{\Re,P}$ denotes the total number of pixels in the κth segment of the jth image and P represents the total number of pixels in the image.

3.3.3 Variance

Variance of the individual segment is computed based on the individual pixel of the segment with respect to the mean of the corresponding segment.

$$F_3^{\kappa,\Re} = \frac{\sum_{b=1}^{P}\left(S_{j,\kappa}^{\Re,P} - \eta\right)}{P} \tag{16}$$

where $S_{j,\kappa}^{\Re,P}$ represents the κth segment belonging to the $\Re$th model of the jth image and η represents the mean of the segment.

3.3.4 Standard deviation

Standard deviation gives a highly accurate idea regarding the distribution of the data, and it is less affected by the extreme values. In other words, it is the best measure of the variation and is based on the calculation of the standard deviation, given as follows:

$$F_4^{\kappa,\Re} = \sqrt{\frac{\sum_{b=1}^{P}\left(S_{j,\kappa}^{\Re,P} - \eta\right)^2}{P-1}} \tag{17}$$

3.3.5 Kurtosis and skewness

Kurtosis is a measure of symmetry and is denoted as $F_5^{\kappa,\Re}$. Skewness is denoted as $F_6^{\kappa,\Re}$. In other words, kurtosis and skewness are the measures of the shape of the object in terms of the numerical value.

3.3.6 Feature ensemble

The features extracted from the segments are represented as

$$F = \left\{F_1^{\kappa,\Re}, F_2^{\kappa,\Re}, \ldots, F_6^{\kappa,\Re}\right\} \tag{18}$$

where $F_1^{\kappa,\Re}, F_2^{\kappa,\Re}, \ldots, F_6^{\kappa,\Re}$ corresponds to the colour histogram, mean, variance, standard deviation, kurtosis and skewness of the segments.

3.4 Leukaemia classification using the proposed Chrono-SCA–based actor-critic neural network

The aim of the actor-critic neural network [26] is to predict the details of the spectral bands as free or occupied. The actor-critic is a learning approach that is composed of actor and critic modules with each module carrying the input layer, the hidden layer and the output layer. The modules are adaptive in nature using the adaptive weights that are obtained using the proposed Chrono-SCA-ACNN algorithm. The input is given to the input layer of the actor module, and the inputs are multiplied with the input weights composed to form the output of the actor layer through the successive computations in the input and hidden layers. The output from the actor layer is fed to the input of the critic layer, and the final output is derived that forms the classified output regarding the occupancy or free spectral bands. Figure 3 shows the architecture of actor-critic neural network, which inherits the reinforcement learning capabilities.

3.4.1 Actor

Actor is the first module in the ACNN; the actor uses a parameterized method, termed as a NN; and the NN with the single hidden layer serves as an actor module. The input to the actor module is the image-based and segment-based features. Thus, the successive computations engaged in the input and hidden layers contribute to the output that forms the input to the critic layer. Thus, the output from the actor layer is represented as

$$A(t) = w^A(t) \times \varepsilon\left(W^A(t) \times F^A(t)\right) \tag{19}$$

$$A(t) = w^A(t) \times \varepsilon^A(t) \tag{20}$$

where $W^A(t)$ is the weight matrix between the input layer and the hidden layer, and $w^A(t)$ denotes the weight matrix between both the layers. The input and the output of the actor layer are denoted as $F^A(T)$ and $A(t)$. The weights of the actor are denoted as $W_1 \in \{w^a(T), W^a(T)\}$. The dimension of the input vector is given as $[(1 \times \kappa) + 4]$, and κ takes the values of r, which is the total number of the eigenvalues obtained using the channel matrix. The activation function is denoted as σ, which is based on the hyperbolic tangent function and is represented as

$$w_1 \in \left\{w^A(t), W^A(t)\right\} \tag{21}$$

The dimension of the input vector is denoted as $[15 + (3 \times \aleph)]$, and $\aleph$ denotes the number of bins.

$$\varepsilon(x) = \frac{e^x - e^{-x}}{e^x + e^{-x}} \tag{22}$$

The activation function is referred to as the hyperbolic tangent function as given in Eq. (22). The activation function $\varepsilon \in [W^A(t)\ F^A(t)]$ is denoted as $\alpha(x)$ for simplicity.

3.4.2 Critic

The critic layer accepts the output from the actor layer along with the inputs of the actor layer to predict the presence of leukaemia. The adaptive weights are used to undergo a smooth prediction with better accuracy. The output from the critic layer is represented as

$$B(t) = w^B(t) \times \varepsilon\left(W^B(t) \cdot F^B(t)\right) \tag{23}$$

$$B(t) = w^B(t) \times \varepsilon^B(t) \tag{24}$$

where $F^B(t) = [F^A(t), A(t)]$, $W^B(t)$ and $w^B(t)$ are the weight matrices between the input and hidden layers and the weight between the hidden and output layers, respectively. The weights of the critic layer are denoted as $w_2 \in \{W^B(t), w^B(t)\}$. The critic layer performs the prediction effectively regarding the presence or absence of the leukaemia in the image.

3.4.3 Proposed Chrono-SCA algorithm

The proposed algorithm is the integration of chronological concept in the Sine Cosine Algorithm [27]. SCA [27] is a population-based optimization algorithm that begins with the generation of random solutions. The random set of solutions is evaluated based on the objective functions, and that is based on the rules followed by the optimization algorithm. The algorithm converges through a series of iterations. Therefore, with the random set of solutions, the probability of determining the global optimal solution increases. The chronological concept is merged in the SCA that imputes the history of the search agent in obtaining the global optimal solution.

Initialization The first step is the initialization that initializes the weights of the network, and the weights are randomly generated.

Evaluate the objective function The objective function is tuned for solving the minimization problem, and the objective function is based on the error of the network. The search agents are evaluated based on the objective function.

Best position update The position of the search agent is denoted as T_P^t, and the best position of the search agent is updated.

Update the parameters The main parameters in SCA are Z_1, Z_2, Z_3 and Z_4, and the parameter Z_1 symbolizes the movement direction; in other words, it indicates the next positions and the

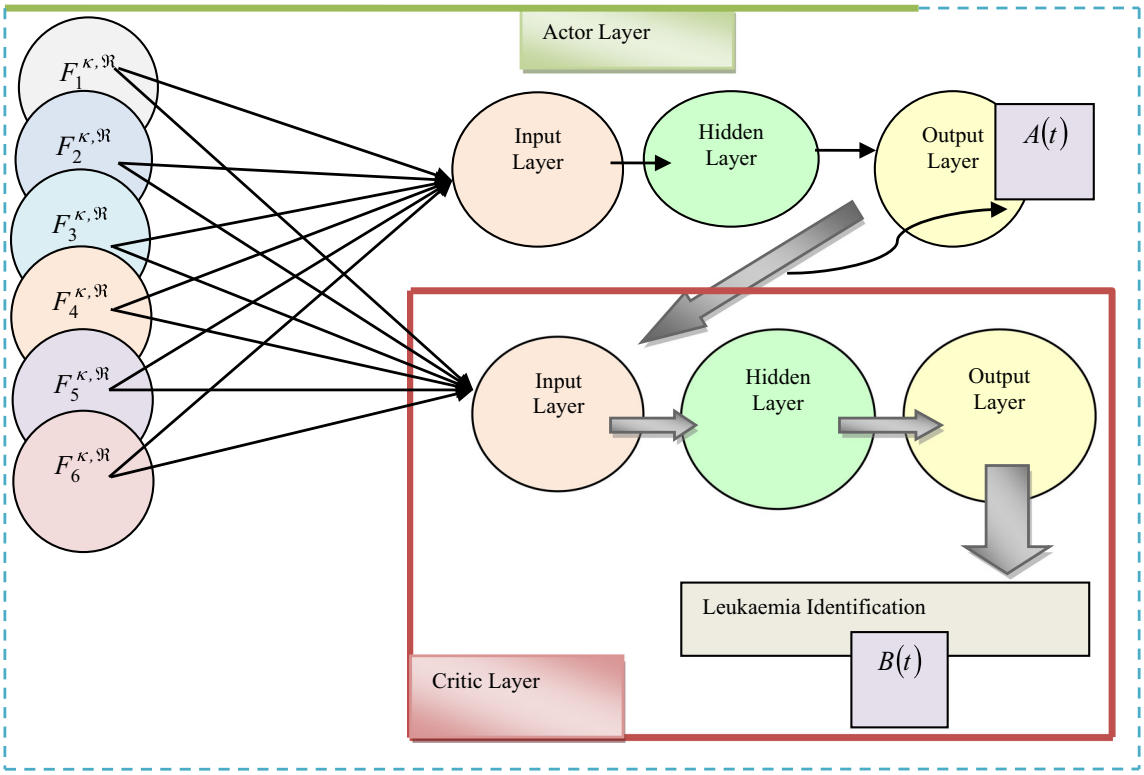

Fig. 3 The architecture of the actor-critic neural network

direction may be either between the source and the destination or outer. The parameter Z_2 defines if the movement is towards or away from the destination. The third random parameter Z_3 defines the random weights for the destination to stochastically emphasize and de-emphasize the desalination impacts that define the distance. The last random parameter (Z_4) switches between the sine and the cosine components. The name SCA is due to the switching between the sine and the cosine components.

Update the position using the proposed Chrono-SCA The position of the search agents is updated, and the position update using the standard SCA is given in Eq. (25) as

$$Y_P^{t+1} = Y_P^t + Z_1 \times \sin(Z_2) \times \left| Z_3 \times T_P^t - Y_P^t \right| \tag{25}$$

where Y_P^t is the position update of the current solution in the Pth dimension at the tth iteration. Z_1, Z_2, Z_3 and Z_4 are the random numbers; T_P^t denotes the position of the destination in the Pth dimension; and || refers to the absolute value. The above equation is rearranged based on an assumption $(T_P^t > Y_P^t)$, as shown in the following:

$$Y_P^{t+1} = Y_P^t + Z_1 \times \sin(Z_2) \times Z_3 \times T_P^t - Y_P^t \times Z_1 \times \sin(Z_2) \tag{26}$$

$$Y_P^{t+1} = Y_P^t \times (1 - Z_1 \times \sin(Z_2)) + Z_1 \times \sin(Z_2) \times Z_3 \times T_P^t \tag{27}$$

The above equation is remodelled as shown in the following:

$$Y_P^t = Y_P^{t-1} \times (1 - Z_1 \times \sin(Z_2)) + Z_1 \times \sin(Z_2) \times Z_3 \times T_P^{t-1} \tag{28}$$

Substituting Eq. (28) for Eq. (27), it gives

$$Y_P^{t+1} = \left[Y_P^{t-1} \times (1 - Z_1 \times \sin(Z_2)) + Z_1 \times \sin(Z_2) \times Z_3 \times T_P^{t-1} \right] \times (1 - Z_1 \times \sin(Z_2)) + Z_1 \times \sin(Z_2) \times Z_3 \times T_P^t \tag{29}$$

The standard equation of SCA is modified using the chronological concept, which takes the average of the position of the search agent derived in Eqs. (27) and (29), as given in the following:

$$Y_P^{t+1} = \frac{Y_P^{t+1} + Y_P^{t+1}}{2} \tag{30}$$

where Y_P^{t+1} is the position of the Pth search agent in the next iteration. Substituting Eqs. (27) and (29) for Eq. (30) gives

$$Y_P^{t+1} = \frac{1}{2} \times \left[\begin{array}{l} Y_P^t \times (1 - Z_1 \times \sin(Z_2)) + Z_1 \times \sin(Z_2) \times Z_3 \times T_P^t + \\ \left[Y_P^{t-1} \times (1 - Z_1 \times \sin(Z_2)) + Z_1 \times \sin(Z_2) \times Z_3 \times T_P^{t-1} \right] \times (1 - Z_1 \times \sin(Z_2)) + \\ Z_1 \times \sin(Z_2) \times Z_3 \times T_P^t \end{array} \right] \tag{31}$$

$$Y_P^{t+1} = \frac{1}{2} \times \begin{bmatrix} Y_P^t \times (1 - Z_1 \times \sin(Z_2)) + Z_1 \times \sin(Z_2) \times Z_3 \times T_P^t + Y_P^{t-1} \times (1 - Z_1 \times \sin(Z_2)) - \\ Z_1 \times \sin(Z_2) \times Y_P^{t-1} \times (1 - Z_1 \times \sin(Z_2)) + Z_1 \times \sin(Z_2) \times Z_3 \times T_P^{t-1} - \\ Z_1^2 \times \sin^2(Z_2) \times Z_3 \times T_P^{t-1} + Z_1 \times \sin(Z_2) \times Z_3 \times T_P^t \end{bmatrix} \tag{32}$$

$$Y_P^{t+1} = \frac{1}{2} \times \begin{bmatrix} Y_P^t \times (1 - Z_1 \times \sin(Z_2)) + Y_P^{t-1} \times (1 - Z_1 \times \sin(Z_2))^2 + \\ Z_1 \times \sin(Z_2) \times Z_3 \times T_P^{t-1} (1 - Z_1 \times \sin(Z_2)) + \\ 2 \times Z_1 \times \sin(Z_2) \times Z_3 \times T_P^t \end{bmatrix} \tag{33}$$

The above equation is employed for position update when the fourth random parameter is less than 0.5. When the random number exceeds 0.5 ($Z_4 \geq 0.5$), the position update is based on Eq. (35).

$$Y_P^{t+1} = Y_P^t + Z_1 \times \cos(Z_2) \times \left| Z_3 \times T_P^t - Y_P^t \right| \tag{34}$$

$$Y_P^{t+1} = \frac{1}{2} \times \begin{bmatrix} Y_P^t \times (1 - Z_1 \times \cos(Z_2)) + Y_P^{t-1} \times (1 - Z_1 \times \cos(Z_2))^2 + \\ Z_1 \times \cos(Z_2) \times Z_3 \times T_P^{t-1} (1 - Z_1 \times \cos(Z_2)) + \\ 2 \times Z_1 \times \cos(Z_2) \times Z_3 \times T_P^t \end{bmatrix} \tag{35}$$

The position of the search agent is updated as

$$Y_P^{t+1} = \begin{cases} \frac{1}{2} \begin{bmatrix} Y_P^t \times (1 - Z_1 \times \sin(Z_2)) + Y_P^{t-1} \times (1 - Z_1 \times \sin(Z_2))(1 - Z_1 \times \sin(Z_2)) + \\ Z_1 \times \sin(Z_2) \times Z_3 \times T_P^{t-1} (1 - Z_1 \times \sin(Z_2)) + \\ 2 \times Z_1 \times \sin(Z_2) \times Z_3 \times T_P^t \end{bmatrix} & ; Z_4 < 0.5 \\ \frac{1}{2} \times \begin{bmatrix} Y_P^t \times (1 - Z_1 \times \cos(Z_2)) + Y_P^{t-1} \times (1 - Z_1 \times \cos(Z_2))^2 + \\ Z_1 \times \cos(Z_2) \times Z_3 \times T_P^{t-1} (1 - Z_1 \times \cos(Z_2)) + \\ 2 \times Z_1 \times \cos(Z_2) \times Z_3 \times T_P^t \end{bmatrix} & ; Z_4 \geq 0.5 \end{cases} \tag{36}$$

where Z_4 is the random number in the range [0, 1].

Terminate The position update is repeated for the maximum number of iterations, and the optimal weights are determined to update the actor-critic neural network. Algorithm 1 shows the pseudocode of the proposed algorithm.

Algorithm 1. Pseudocode of the proposed ChronoSCA

4 Results and discussion

The section deliberates the results and discussion of the proposed method, and the comparative analysis of the method describes the effectiveness of the proposed method of leukaemia classification.

4.1 Experimental setup

The experimentation is performed using the computer system of Windows 8 OS with 4 GB RAM, and the implementation is performed in the MATLAB.

Proposed Chrono-SCA for tuning the optimal weights	
1	**Input :** Population, Y_P ; $(1 \leq P \leq I)$
2	**Output:** Best position, Y_P^{t+1}.
3	Initialization
4	Do
5	Evaluate the search agents based on the objective function
6	Update the best position
7	Update the random parameters Z_1, Z_2, Z_3, and Z_4.
8	*if* $(T_P^t > Y_p^t)$
9	{
10	Update the position of the search agents based on equation (33).
11	*Elseif* $(Z_3\, T_P^t > Y_P^t)$
12	Update the position of the search agents based on equation (35).
13	}
14	While $(t < t_{max})$
15	Return the best solution.
16	End

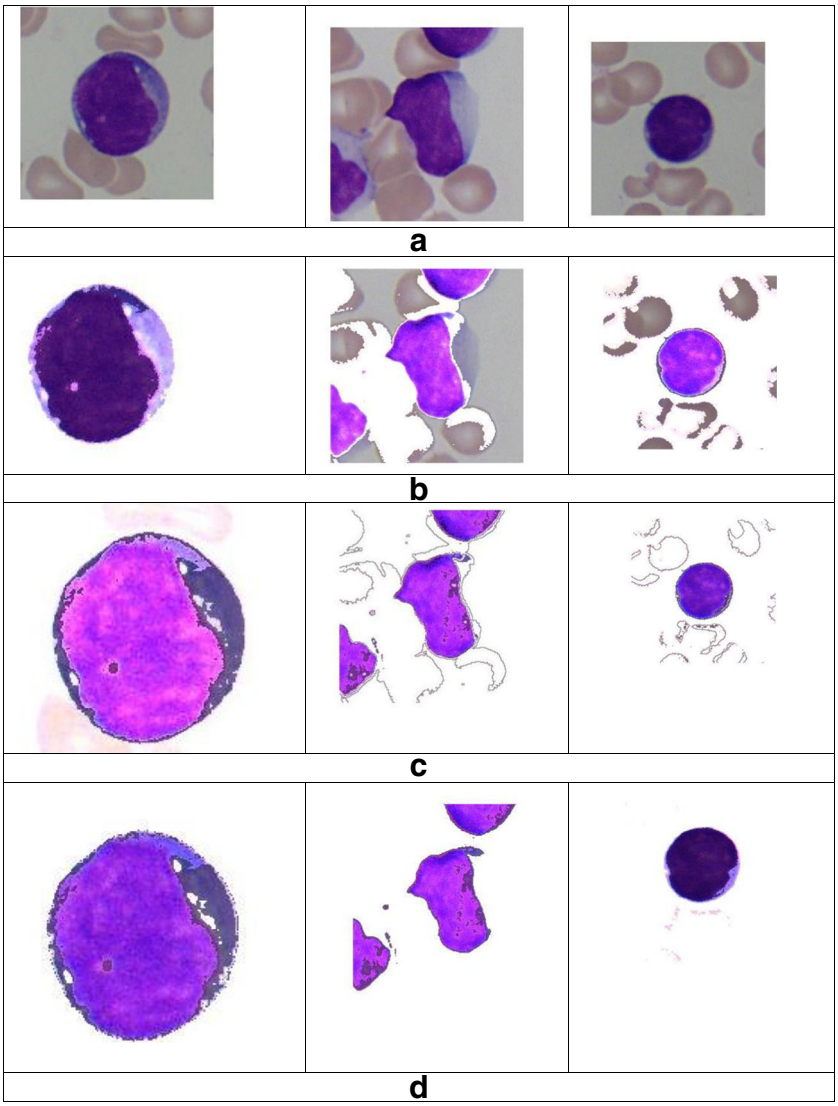

Fig. 4 Sample results of the experiment. **a** Input images. **b** Segmentation using active contour. **c** Segmentation using FCM. **d** Segmentation using a hybrid model

4.2 Dataset description

The experimentation is performed using the ALL-IDB2 database [16]. The ALL-IDB2 (version 1.0) consists of the cropped area of significance that carries the normal and blast cells. This dataset contains 108 images. ALL-IDB2 images have similar grey-level properties to the images of the ALL-IDB1, except the image dimensions.

4.3 Experimental results

Figure 4 depicts the sample results of the experiment. The sample input images are depicted in Fig. 4 a. The segmentation results using the active contour of the input images are depicted in Fig. 4 b, and the segmentation results using the FCM are depicted in Fig. 4 c. Finally, the segmentation of the hybrid model for the images in Fig. 4 a is depicted in Fig. 4 d.

4.4 Performance metrics

The performance of the proposed classification method is evaluated using three metrics, such as accuracy, sensitivity and specificity.

4.4.1 Accuracy

It is the measure of correctness of the detection, given as

$$\mathrm{ACC} = \frac{\mathrm{TP} + \mathrm{TN}}{\mathrm{TP} + \mathrm{FP} + \mathrm{FN} + \mathrm{TN}} \tag{37}$$

where TP is a true positive, TN is a true negative, FN is a false negative and FP is a false positive.

4.4.2 Sensitivity (true positive rate)

The sensitivity or the true positive rate (TPR) is defined as the number of positives identified correctly.

$$\mathrm{TPR} = \frac{\mathrm{TP}}{\mathrm{TP} + \mathrm{FN}} \tag{38}$$

4.4.3 Specificity (true negative rate)

The specificity or the true negative rate (TNR) is defined as the number of negatives identified correctly.

$$\mathrm{TNR} = \frac{\mathrm{TN}}{\mathrm{TN} + \mathrm{FP}} \tag{39}$$

4.5 Methods taken for the comparison

The methods taken for the comparison include hybrid segmentation + NN [18], hybrid segmentation + concurrent NN [3], threshold segmentation + *k*-nearest neighbour (KNN) [9], hybrid segmentation + random forest [8] and hybrid segmentation + ACNN [26] for the comparison with the proposed hybrid segmentation + Chrono-SCA-ACNN.

4.6 Performance analysis

The section shows the performance analysis of the proposed method of leukaemia detection.

4.6.1 Performance based on training percentage

Figure 5 shows the performance analysis of the proposed method based on the training percentage. The analysis is progressed with the training percentages, denoted as *k*, from 0.4 to 0.85 and for the iteration number from 20 to 100. The analysis of the proposed method based on TPR is depicted in Fig. 5 a. When k = 0.4, the TPR of Chrono-SCA-ACNN during the iteration numbers 20, 40, 60, 80 and 100 is 0.88, 1, 0.5, 0.5 and 0.5, respectively. The TPR of the proposed method keeps in increasing with the increase in the iteration number. Similarly, when k = 0.85, the TPR of Chrono-SCA-ACNN during the iteration numbers 20, 40, 60, 80 and 100 is 1, respectively. The analysis of the proposed method based on TNR is depicted in Fig. 5 b. When k = 0.4, the TNR of Chrono-SCA-ACNN during the iteration numbers 20, 40, 60, 80 and 100 is 0.5, respectively. The TNR of the proposed method keeps in increasing with the increase in the iteration number. Similarly, when k = 0.85, the TPR of Chrono-SCA-

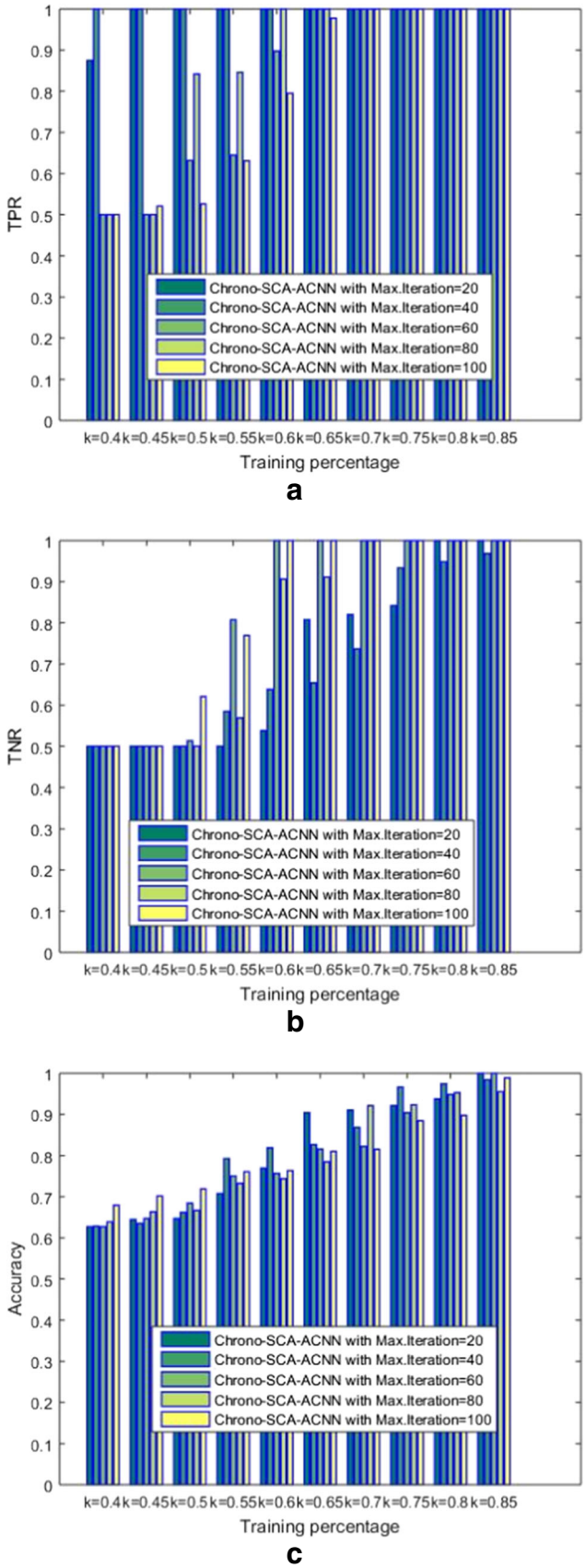

Fig. 5 Performance analysis based on training percentage. **a** TPR. **b** TNR. **c** Accuracy

ACNN during the iteration numbers 20, 40, 60, 80 and 100 is 1, 0.97, 1, 1 and 1, respectively. The analysis of the proposed method based on accuracy is depicted in Fig. 5 c. When k = 0.4, the accuracy of Chrono-SCA-ACNN during the iteration numbers 20, 40, 60, 80 and 100 is 0.63, 0.63, 0.63, 0.64 and 0.68, respectively. The accuracy of the proposed method keeps on increasing with the increase in the iteration number. Similarly, when the training percentage is 0.85, the accuracy of Chrono-SCA-ACNN during the iteration numbers 20, 40, 60, 80 and 100 is 1, 0.98, 1, 0.96 and 0.99, respectively.

4.6.2 Performance based on *k*-fold validation

Figure 6 shows the performance analysis of the proposed method based on the k-cross fold validation. The analysis is progressed with the cross-fold values, denoted as kf, from 5 to 10 and for the iteration number from 20 to 100. The analysis of the proposed method based on TPR is depicted in Fig. 6 a. When kf = 5, the TPR of Chrono-SCA-ACNN during the iteration numbers 20, 40, 60, 80 and 100 is 0.65, 0.62, 0.70, 0.83 and 0.84, respectively. The TPR of the proposed method keeps in increasing with the increase in the iteration number. Similarly, when kf = 10, the TPR of Chrono-SCA-ACNN during the iteration numbers 20, 40, 60, 80 and 100 is 0.90, 0.89, 0.89, 0.93 and 0.95, respectively. The analysis of the proposed method based on TNR is depicted in Fig. 6 b. When kf = 5, the TNR of Chrono-SCA-ACNN during the iteration numbers 20, 40, 60, 80 and 100 is 0.88, 0.86, 0.72, 0.70 and 0.71, respectively. The TNR of the proposed method keeps increasing with the increase in the iteration number. Similarly, when kf = 10, the TPR of Chrono-SCA-ACNN during the iteration numbers 20, 40, 60, 80 and 100 is 1, 1, 0.89, 0.89 and 0.92, respectively. The analysis of the proposed method based on accuracy is depicted in Fig. 6 c. When kf = 5, the accuracy of Chrono-SCA-ACNN during the iteration numbers 20, 40, 60, 80 and 100 is 0.79, 0.74, 0.75, 0.78 and 0.77, respectively. The accuracy of the proposed method keeps on increasing with the increase in the iteration number. Similarly, when kf = 10, the accuracy of Chrono-SCA-ACNN during the iteration numbers 20, 40, 60, 80 and 100 is 0.87, 0.86, 0.87, 0.87 and 0.86, respectively.

4.7 Comparative analysis

This section deliberates the analysis using the comparative methods based on the performance metrics.

4.7.1 Based on training percentage

Figure 7 shows the comparative analysis of the leukaemia detection methods with respect to the training percentage. The analysis of TPR is depicted in Fig. 7 a. When k = 0.4, the TPR of hybrid segmentation + NN, hybrid segmentation +

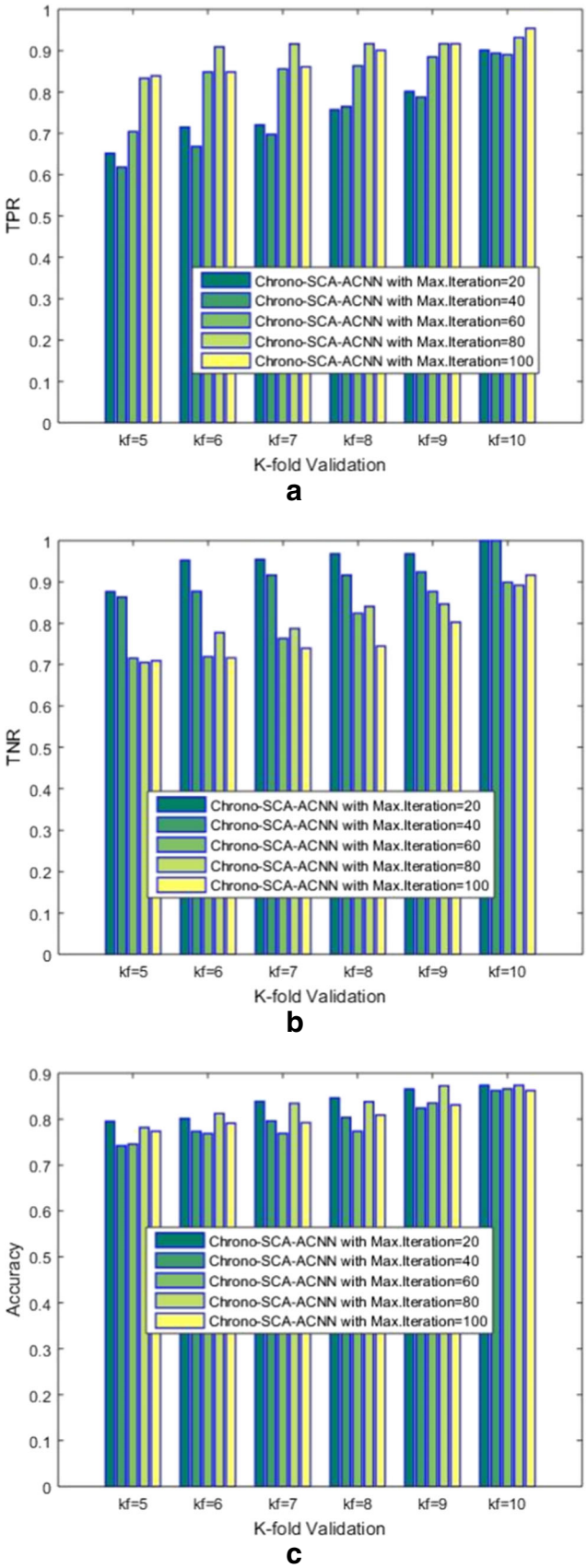

Fig. 6 Performance analysis based on k-fold validation. **a** TPR. **b** TNR. **c** Accuracy

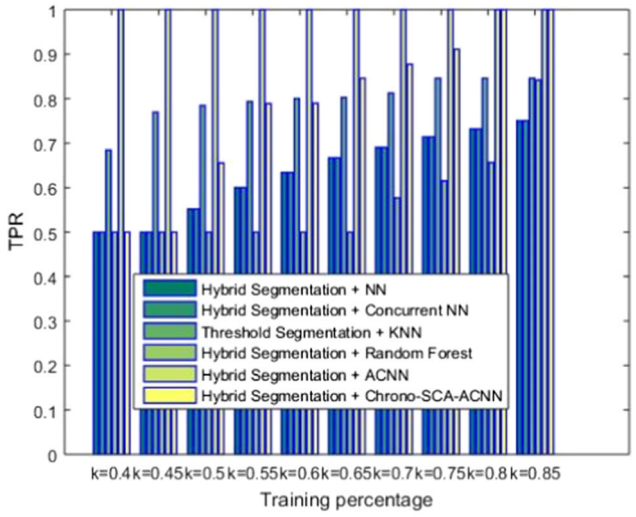

a

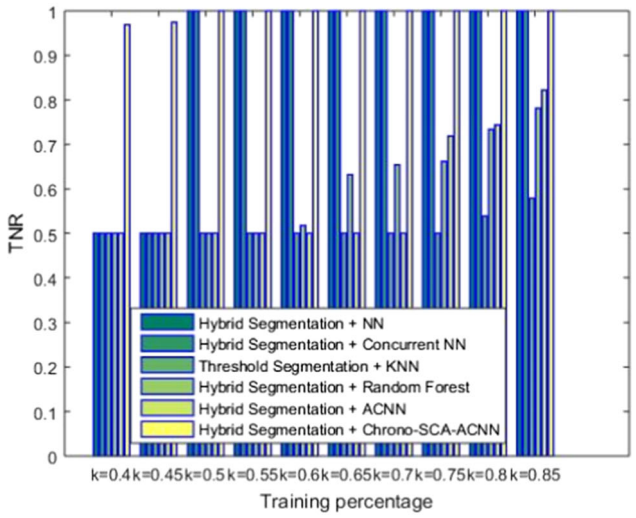

b

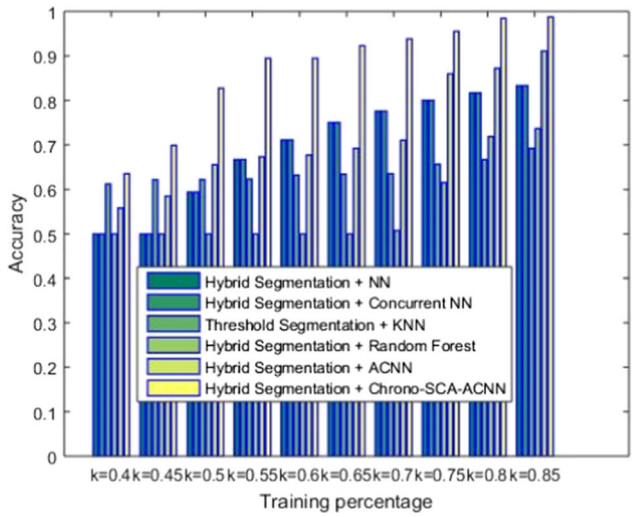

c

Fig. 7 Comparative analysis based on the training percentage. **a** TPR. **b** TPR. **c** Accuracy

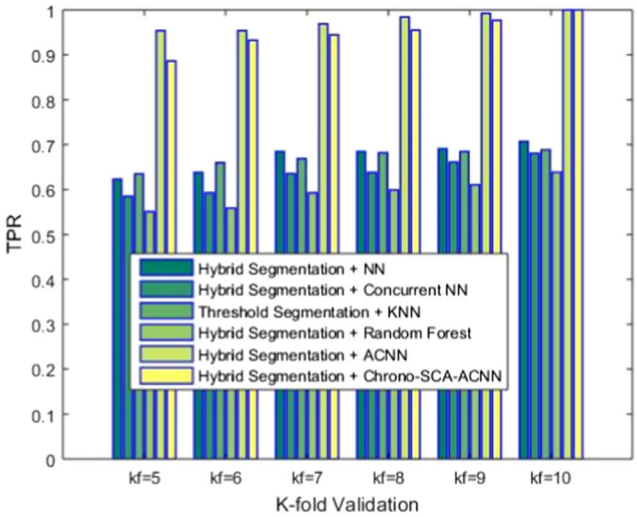

a

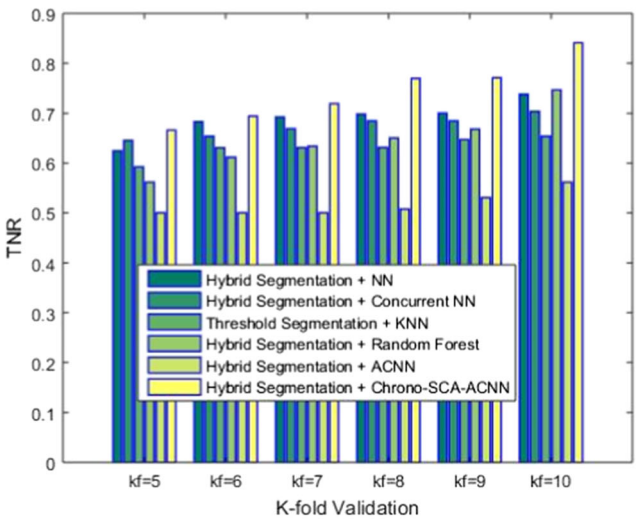

b

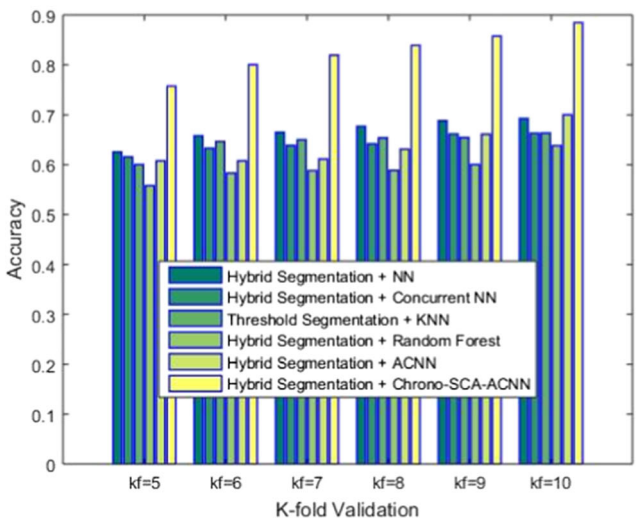

c

Fig. 8 Comparative analysis based on the *k*-fold validation. **a** TPR. **b** TPR. **c** Accuracy

Table 1 Comparative analysis of the leukaemia detection methods

Methods	Accuracy	Sensitivity	Specificity
Hybrid segmentation + NN	0.83	1	0.75
Hybrid segmentation + concurrent NN	0.83	1	0.75
Threshold segmentation + KNN	0.69	0.58	0.85
Hybrid segmentation + random forest	0.74	0.78	0.84
Hybrid segmentation + ACNN	0.91	0.82	1
Proposed hybrid segmentation + Chrono-SCA-ACNN	*0.99*	*1*	*1*

The values specified in italic represent the best performance

concurrent NN, threshold segmentation + KNN, hybrid segmentation + random forest, hybrid segmentation + ACNN and hybrid segmentation + Chrono-SCA-ACNN is 0.5, 0.5, 0.68, 0.5, 1 and 0.5, respectively. Similarly, when $k = 0.85$, the TPR of chrono hybrid segmentation + NN, hybrid segmentation + concurrent NN, threshold segmentation + KNN, hybrid segmentation + random forest, hybrid segmentation + ACNN and hybrid segmentation + Chrono-SCA-ACNN is 0.75, 0.75, 0.85, 0.84, 1 and 1, respectively. The analysis of the proposed method based on TNR is depicted in Fig. 7 b. When $k = 0.4$, the TNR of hybrid segmentation + NN, hybrid segmentation + concurrent NN, threshold segmentation + KNN, hybrid segmentation + random forest, hybrid segmentation + ACNN and hybrid segmentation + Chrono-SCA-ACNN is 0.5, 0.5, 0.5, 0.5, 0.5 and 0.97, respectively. When the training percentage is 0.85, the TPR of hybrid segmentation + NN, hybrid segmentation + concurrent NN, threshold segmentation + KNN, hybrid segmentation + random forest, hybrid segmentation + ACNN and hybrid segmentation + Chrono-SCA-ACNN is 1, 1, 0.58, 0.78, 0.82 and 1, respectively. The analysis of the proposed method based on accuracy is depicted in Fig. 7 c. When $k = 0.4$, the accuracy of hybrid segmentation + NN, hybrid segmentation + concurrent NN, threshold segmentation + KNN, hybrid segmentation + random forest, hybrid segmentation + ACNN and hybrid segmentation + Chrono-SCA-ACNN is 0.5, 0.5, 0.61, 0.5, 0.56 and 0.63, respectively. The accuracy of the proposed method keeps on increasing with the increase in the *k*-fold. When the training percentage is 0.85, the accuracy of hybrid segmentation + NN, hybrid segmentation + concurrent NN, threshold segmentation + KNN, hybrid segmentation + random forest, hybrid segmentation + ACNN and hybrid segmentation + Chrono-SCA-ACNN is 0.83, 0.83, 0.69, 0.74, 0.91 and 0.99, respectively. The proposed method outperforms the existing methods in terms of accuracy, specificity and sensitivity.

4.7.2 Based on the *k*-fold validation

Figure 8 shows the comparative analysis of the leukaemia detection methods with respect to the training percentage. The analysis of TPR is depicted in Fig. 8 a. When $kf = 5$, the TPR of hybrid segmentation + NN, hybrid segmentation + concurrent NN, threshold segmentation + KNN, hybrid segmentation + random forest, hybrid segmentation + ACNN and hybrid segmentation + Chrono-SCA-ACNN is 0.62, 0.58, 0.63, 0.55, 0.95 and 0.89, respectively. Similarly, when $kf = 10$, the TPR of chrono hybrid segmentation + NN, hybrid segmentation + concurrent NN, threshold segmentation + KNN, hybrid segmentation + random forest, hybrid segmentation + ACNN and hybrid segmentation + Chrono-SCA-ACNN is 0.71, 0.68, 0.69, 0.64, 1 and 1, respectively. The analysis of the proposed method based on TNR is depicted in Fig. 8 b. When $kf = 5$, the TNR of hybrid segmentation + NN, hybrid segmentation + concurrent NN, threshold segmentation + KNN, hybrid segmentation + random forest, hybrid segmentation + ACNN and hybrid segmentation + Chrono-SCA-ACNN is 0.62, 0.65, 0.59, 0.56, 0.5 and 0.67, respectively. When $kf = 10$, the TPR of hybrid segmentation + NN, hybrid segmentation + concurrent NN, threshold segmentation + KNN, hybrid segmentation + random forest, hybrid segmentation + ACNN and hybrid segmentation + Chrono-SCA-ACNN is 0.74, 0.70, 0.65, 0.75, 0.56 and 0.84, respectively. The analysis of the proposed method based on accuracy is depicted in Fig. 8 c. When the training percentage is 5, the

Table 2 Analysis based on complexity

Methods	Features	Accuracy (%)	Computational time (s)
Weighted KNN	271	99.9	520
Cubic KNN	271	99.9	86
Ensemble boosted trees	271	99.9	1200
Proposed hybrid segmentation + Chrono-SCA-ACNN	132	99	15

accuracy of hybrid segmentation + NN, hybrid segmentation + concurrent NN, threshold segmentation + KNN, hybrid segmentation + random forest, hybrid segmentation + ACNN and hybrid segmentation + Chrono-SCA-ACNN is 0.63, 0.62, 0.6, 0.56, 0.61 and 0.76, respectively. The accuracy of hybrid segmentation + NN, hybrid segmentation + concurrent NN, threshold segmentation + KNN, hybrid segmentation + random forest, hybrid segmentation + ACNN and hybrid segmentation + Chrono-SCA-ACNN when $kf = 0.85$ is 0.69, 0.66, 0.66, 0.64, 0.7 and 0.88, respectively. The proposed method outperforms the existing methods in terms of accuracy, specificity and sensitivity.

4.8 Comparative analysis

Table 1 shows the comparative analysis of the proposed method of leukaemia detection based on performance metrics. The methods hybrid segmentation + NN, hybrid segmentation + concurrent NN, threshold segmentation + KNN, hybrid segmentation + random forest, hybrid segmentation + ACNN and hybrid segmentation + Chrono-SCA-ACNN attained an accuracy of 0.83, 0.83, 0.69, 0.74, 0.91 and 0.99, respectively. The sensitivity of the methods hybrid segmentation + NN, hybrid segmentation + concurrent NN, threshold segmentation + KNN, hybrid segmentation + random forest, hybrid segmentation + ACNN and hybrid segmentation + Chrono-SCA-ACNN is 1, 1, 0.58, 0.78, 0.82 and 1, respectively. Similarly, the specificity of the methods hybrid segmentation + NN, hybrid segmentation + concurrent NN, threshold segmentation + KNN, hybrid segmentation + random forest, hybrid segmentation + ACNN and hybrid segmentation + Chrono-SCA-ACNN is 0.75, 0.75, 0.85, 0.84, 1 and 1, respectively. Thus, it is clear that the proposed method acquired better results.

4.9 Scalability analysis

Table 2 shows the analysis based on the complexity. Here, the existing methods, such as weighted KNN [28], cubic KNN [28] and ensemble boosted tree [28], have the computational time of 520 s, 86 s and 1200 s, respectively. Also, these methods have the accuracy of 99.9%. On the other hand, the proposed hybrid segmentation + Chrono-SCA-ACNN has an accuracy and computational time of 99% and 15 s, respectively. When the number of features increases, the computational time increases. Here, the existing methods use more number of features and have high computational time, while the proposed method uses a minimum number of features and has the minimum computational time. However, the proposed method obtains the accuracy of 90%, which indicates good performance.

5 Conclusion

This paper proposes the method for leukaemia classification using the Chrono-SCA–based ACNN. The classification is progressed through segmenting the cytoplasm and nucleus of the image. Initially, the blood smear images are preprocessed and applied to the proposed entropy-based hybrid model, which extracts the image-level features and statistical features from the segments. Then, the selected features are applied to the proposed Chrono-SCA–based ACNN, which detects the leukaemia. At last, the experimentation is performed using the ALL-IDB2 database, and the effectiveness of the proposed method over the existing methods is evaluated. Experimentation using the ALL-IDB2 database proves the effectiveness of the proposed method, yielding a better classification accuracy of 0.99. The analysis of the proposed method of classification conveys that the proposed method outperforms the existing classification methods. In the future, we will develop the hybrid optimization algorithm to train the ACNN to further increase the classification performance. Also, we will develop a technique for leukaemia classification to obtain the maximum accuracy (99.9%) with minimum numbers of features.

References

1. Oikonomidis I, Kyriazi N, Argyros AA (2011) Efficient model-based 3D tracking of hand articulations using Kinect. In: Proceedings of the 22nd British Machine Vision Conference on University of Dundee (BMVC), 29 August–2 September 2011
2. Palumbo P, Miconi G, Cinque B, Lombardi F, La Torre C, Dehcordi SR, Galzio R, Cimini A, Giordano A, Cifone MG (2017) NOS2 expression in glioma cell lines and glioma primary cell cultures: correlation with neurosphere generation and SOX-2 expression. Oncotarget 8(15)
3. Zhao J, Zhang M, Zhou Z, Chu J, Cao F (2017) Automatic detection and classification of leukocytes using convolutional neural networks. Med Biol Eng Comput 55(8):1287
4. Ding Y, John NW, Smith L, Sun JA, Smith M (2015) Combination of 3D skin surface texture features and 2D ABCD features for improved melanoma diagnosis. Med Biol Eng Comput 53(10): 961–974
5. Cinque B, La Torre C, Lombardi F, Palumbo P, Evtoski Z, Santini SJ, Falone S, Cimini A, Amicarelli F, Cifone MG (2017) VSL# 3 probiotic differently influences IEC-6 intestinal epithelial cell status and function. J Cell Physiol 232(12):3530–3539
6. Guadagni S, Fiorentini G, Clementi M, Palumbo G, Masedu F, Deraco M, De Manzoni G, Chiominto A, Valenti M, Pellegrini C (2017) MGMT methylation correlates with melphalan pelvic perfusion survival in stage III melanoma patients: a pilot study. Melanoma Res 27(5)
7. Sista F, Abruzzese V, Clementi M, Guadagni S, Montana L, Carandina S (2018) Resolution of type 2 diabetes after sleeve gastrectomy: a 2-step hypothesis. Surg Obes Relat Dis 14(3):284–290
8. Mishra S, Majhi B, Sa PK, Sharma L (2017) Gray level co-occurrence matrix and random forest based acute lymphoblastic leukemia detection. Biomed Signal Process Control 33:272–280

9. Li Y, Zhu R, Mi L, Cao Y, Yao D (2016) Segmentation of white blood cell from acute lymphoblastic leukemia images using dual-threshold method. Comput Math Methods Med
10. Fatichah C, Tangel ML, Widyanto MR, Dong F, Hirota K (2012) Interest-based ordering for fuzzy morphology on white blood cell image segmentation. J Adv Comput Intell Intell Inform 16(1):76–86
11. Huang HQ, Fang XZ, Shi J, Hu J (2014) Abnormal localization of immature precursors (ALIP) detection for early prediction of acute myelocytic leukemia (AML) relapse. J Med Biol Eng Comput 52(2):121–129
12. Sezgin M (2004) Survey over image thresholding techniques and quantitative performance evaluation. J Electron Imaging 13(1): 146–168
13. Nallaperumal K, Krishnaveni K (2008) Watershed segmentation of cervical images using multiscale morphological gradient and HSI color space. Int J Imaging Sci Eng:212–216
14. Agaian S, Madhukar M, Chronopoulos AT (2014) Automated screening system for acute myelogenous leukemia detection in blood microscopic images. IEEE Syst J 8(3):995–1004
15. Fiehn A-MK, Engel U, Holck S, Munck LK, Engel PJH (2016) CD3 immunohistochemical staining in diagnosis of lymphocytic colitis. Hum Pathol 48:25–31
16. ALL IDB Database. https://homes.di.unimi.it/scotti/all/. Accessed on November 2017
17. Oikonomidis I, Kyriazis N, Argyros, AA (2011) Full DOF tracking of a hand interacting with an object by modeling occlusions and physical constraints. In: Proceedings of the International Conference on Computer Vision ICCV, pp 2088–2095
18. Khashman A, Abbas HH (2013) Acute lymphoblastic leukemia identification using blood smear images and a neural classifier. In: Proceedings of the International Work-Conference on Artificial Neural Networks (IWANN), Advances in Computational Intelligence, pp 80–87
19. Rawat J, Singh A, Bhadauria HS, Virmani J, Devgun JS (2017) Classification of acute lymphoblastic leukaemia using hybrid hierarchical classifiers. Multimed Tools Appl 76(18):19057–19085
20. Bhattacharjee R, Saini LM (2015) Robust technique for the detection of acute lymphoblastic leukemia. In: Proceedings of the IEEE Power, Communication and Information Technology Conference (PCITC), pp 657–662
21. Blood and Marrow Stem Cell Transplantation, Leukaemia and Lymphoma Society (2015) https://www.mskcc.org/cancer-care/diagnosis-treatment/cancer-treatments/blood-stem-cell-transplantation
22. Srisukkham W, Zhang L, Neoh SC, Todryk S, Lim CP (2017) Intelligent leukaemia diagnosis with bare-bones PSO based feature optimization. Appl Soft Comput 56:405–419
23. Viswanathan P (2015) Fuzzy C means detection of leukemia based on morphological contour segmentation. Procedia Comput Sci 58: 84–90
24. Ali K, Nadi S (2010) An implementation of the active contours without edges model and the logic framework for active contours on multi-channel images
25. Sergyan S (2008) Color histogram features based image classification in content-based image retrieval systems. In: Proceedings of the 6th International Symposium on Applied Machine Intelligence and Informatics, pp 221–224
26. Zhao D, Wang B, Liu D (2013) A supervised actor–critic approach for adaptive cruise control. Soft Comput 17(11):2089–2099
27. Mirjalili S (2016) SCA: a Sine Cosine Algorithm for solving optimization problems. Knowl-Based Syst 96:120–133
28. Arya M (2019) Automated detection of acute leukemia using K-means clustering algorithm

Krishna Kumar Jha received a B. Sc. degree from University of Calcutta, India; Master in Computer Application (MCA) from Sikkim Manipal University of Health, Medical & Technological Sciences, Gangtok, India; and Master of Technology–Computer Science and Application from University of Calcutta, India. He is pursuing Ph. D. in Technology from Maulana Abul Kalam Azad University of Technology, Kolkata, India. He is presently working as Assistant Professor at MCA Department of Calcutta Institute of Technology, Howrah, West Bengal, India. His research areas include medical image processing and big data. He has published more than 4 research papers in various international journals and conferences and reviewed papers for reputed journals.

Himadri Sekhar Dutta received his B. Tech degree in Electronics and Communication Engineering from Kalyani Government Engineering College (Kalyani, India), M. Tech. degree in Optics and Opto-Electronics from University of Calcutta (Kolkata, India), and Ph. D. in Technology from Institute of Radio Physics and Electronics (Kolkata, India), respectively. He is presently working as Assistant Professor at the ECE Department of Kalyani Government Engineering College, Kalyani. He was the Chairperson of IEEE Young Professional, Kolkata Section, for two consecutive years (in 2016 and 2017) and actively participated in different activities conducted by IEEE. His research areas include medical image processing, embedded systems and opto-electronic devices. He has published more than 70 research papers in various international journals and conferences and reviewed papers for reputed journals and international conferences.